

Time evolution of superradiant instabilities for charged black holes in a cavity

Juan Carlos Degollado^{1,*} and Carlos A. R. Herdeiro^{1,†}

¹ *Departamento de Física da Universidade de Aveiro and I3N,
Campus de Santiago, 3810-183 Aveiro, Portugal.*

(Dated: December 2013)

Frequency domain studies have recently demonstrated that charged scalar fields exhibit fast growing superradiant instabilities when interacting with charged black holes in a cavity. Here, we present a time domain analysis of the long time evolution of test charged scalar field configurations on the Reissner-Nordström background, with or without a mirror-like boundary condition. Initial data is taken to be either a Gaussian wave packet or a regularised (near the horizon) quasi-bound state. Then, Fourier transforming the data obtained in the evolution confirms the results obtained in the frequency domain analysis, in particular for the fast growing modes. We show that spherically symmetric ($\ell = 0$) modes have even faster growth rates than the $\ell = 1$ modes for ‘small’ field charge. Thus, our study confirms that this setup is particularly promising for considering the non-linear development of the superradiant instability, since the fast growth makes the signal overcome the numerical error that dominates for small growth rates, and the analysis may be completely done in spherical symmetry.

PACS numbers: 95.30.Sf, 04.70.Bw, 04.40.Nr, 04.25.dg

I. INTRODUCTION

Superradiant scattering is a classical process through which energy can be extracted from a black hole (BH). For a rotating, i.e Kerr, BH, with horizon angular velocity Ω_+ , this process occurs when an impinging wave of a bosonic field with frequency ω and azimuthal quantum number m obeys the condition $\omega < m\Omega_+$ [1–6]. Then, upon scattering, rotational energy is extracted from the BH, simultaneously extracting enough angular momentum such that the BH’s area/entropy does not decrease. This scattering can become an instability if the wave repeatedly scatters off the BH. This is achieved, for instance, by either introducing a mass term for the field or imposing a mirror-like boundary condition outside the BH, which reflects the wave. Then, the total extracted energy grows exponentially with time - suggesting an explosive phenomenon that has been dubbed the *black hole bomb* [3, 7] -, and the linear (test field) approximation will break down. The complete non-linear development of this instability, including its back-reaction on the geometry and its endpoint, is still not understood. It has been suggested that the explosive event may be akin to a *bose nova* [8] observed in condensed matter systems, and further progress needs fully non-linear numerical simulations [9]. One problem in achieving these numerical evolutions is that the growth rate of the instability is very small [5, 10–15] and its signal can become buried in numerical noise.

In a recent work [16] we have shown the growth rate of scalar superradiant modes can be much faster in the case of a charged, i.e Reissner-Nordström (RN), BH. In

this case, superradiant scattering occurs if a charged field with frequency ω and charge q impinging on a charged BH with horizon electric potential Φ_+ obeys $\omega < \omega_c \equiv q\Phi_+$ [17]. Upon scattering, Coulomb energy is extracted from the BH, simultaneously decreasing enough its charge such that its area/entropy does not decrease. In this case, however, in order to have a superradiant instability it is not enough to add a mass term to the field. It is also necessary to impose a mirror-like boundary condition at some distance from the BH [18–21]. For such charged BH in a cavity, states with an imaginary part of the frequency of up to $\text{Im}(M\omega) \sim 0.07$ were obtained in [16]. As a comparison, in the Kerr case, the maximum growth rates are $\text{Im}(M\omega) \sim 1.74 \times 10^{-7}$ for massive fields in asymptotically Minkowski space and $\text{Im}(M\omega) \sim 6 \times 10^{-5}$ for mirror-like boundary conditions [5, 15]. The growth time scale is set by the inverse of $\text{Im}(\omega)$. Therefore the aforementioned frequencies demonstrate that the e-folding time can be at least three orders of magnitude smaller in the charged case than in the rotating case. Subsequently, it was argued in [22] that, for the charged case, $\text{Im}(M\omega)$ scales as qQ/r_+ , for large qQ , where Q, r_+ are the charge and (Schwarzschild) radial coordinate of the BH’s event horizon. Such scaling implies that in the charged case, the instability’s e-folding time can be made arbitrarily short by increasing q .

In this paper, by performing a time domain analysis, we further confirm the existence of fast growing superradiant modes for charged BHs in a cavity. We evolve in time two types of charged scalar field wave packets, in the background of a RN BH in a cavity with radius r_m . The choice of the initial data, as well as background and field parameters determines the particular set of quasi-bound states that will have leading amplitudes. By time evolving this initial data and Fourier transforming the evolution data, we identify the frequencies of these dominant quasi-bound states, and observe they match values

*Electronic address: jcdaza@ua.pt

†Electronic address: herdeiro@ua.pt

obtained in the frequency domain analysis [16], some of which correspond to unstable modes. After a sufficiently long time evolution, we verify that the unstable mode with the largest growth rate dominates the evolution and its growth rate is in excellent agreement with the imaginary part obtained from the frequency domain analysis.

In [16] we have focused on modes with angular momentum number $\ell = 1$. This choice was motivated by the goal of comparison with the rotating case, for which these modes are the fastest growing ones. Here, we shall also explicitly consider $\ell = 0$ modes and observe that similar instabilities to the $\ell = 1$ case - which may have even faster growth rates for ‘small’ field charge - are obtained. By contrast, in the rotating case, modes with $\ell = 0$ cannot yield superradiant states. The existence of unstable spherically symmetric modes for the charged case implies that the non-linear development of the superradiant instability can be studied in a spherically symmetric setup. Such symmetry, together with the shorter time scales involved, makes charged BHs in a cavity particularly interesting for non-linear studies of the superradiant instability.

One may worry, however, that numerical difficulties will be introduced by the need to impose a mirror-like boundary condition. Indeed, in [23], for instance, an attempt to impose such boundary conditions for a binary BH evolution led to loss of convergence after a few reflections of the signal off the reflecting boundary. We will find no such problem: our implementation of the mirror-like boundary condition yields long term stable evolutions, as in [15], for the test field analysis performed herein.

This paper is organized as follows. In Sec. II we describe the background and field setup. In Sec. III we discuss the test field’s flux and energy which shall be monitored during the time evolutions, the system of equations to be solved in the time domain analysis, the boundary conditions and the numerical method. In Sec. IV the numerical results for two types of initial data are described. We also review some results on quasi-bound states of charged scalar fields around charged BHs with or without mirror-like boundary conditions. In the following, the former states shall be dubbed *mirrored states*. Final remarks are presented in Sec. V. We shall use units in which $G = 1 = c = \hbar$.

II. FRAMEWORK

We consider Einstein-Maxwell theory minimally coupled to a complex, charged, massive scalar field. Linearizing the field equations (on the scalar field), yield the Einstein-Maxwell equations plus the Klein-Gordon equation describing the evolution of massive charged scalar perturbation in the Einstein-Maxwell background:

$$(\nabla_\nu - iqA_\nu)(\nabla^\nu - iqA^\nu)\Phi - \mu^2\Phi = 0, \quad (1)$$

where A_ν is the electromagnetic potential and q and μ are the charge and the mass of the scalar field.

The Einstein-Maxwell background we wish to consider is the RN black hole. The metric, written in standard Schwarzschild type coordinates $(\tilde{t}, r, \theta, \phi)$ reads

$$ds^2 = -f(r)d\tilde{t}^2 + \frac{dr^2}{f(r)} + r^2(d\theta^2 + \sin^2\theta d\phi^2), \quad (2)$$

where

$$f(r) = \frac{(r - r_+)(r - r_-)}{r^2}, \quad r_\pm \equiv M \pm \sqrt{M^2 - Q^2}, \quad (3)$$

whereas the gauge field is given by an electric potential of the form $A_\nu dx^\nu = -Q/r d\tilde{t}$.

The Klein-Gordon equation (1) is separable in the RN geometry with the ansatz

$$\Phi(\tilde{t}, r, \theta, \phi) = \sum_{\ell, m} e^{-i\omega\tilde{t}} Y_\ell^m(\theta, \phi) \phi_\ell(r), \quad (4)$$

where $Y_\ell^m(\theta, \phi)$ are the scalar spherical harmonics satisfying $\Delta_{S^2} Y_\ell^m(\theta, \phi) = -\ell(\ell + 1) Y_\ell^m(\theta, \phi)$. A Schrödinger-like radial equation is then obtained for a new radial function $R_\ell(r) = r\phi_\ell(r)$:

$$\left[-\frac{d^2}{dr^{*2}} + V(r) \right] R_\ell(r) = \omega^2 R_\ell(r), \quad (5)$$

where the effective potential is given by

$$V(r) = \frac{2qQ\omega}{r} - \frac{q^2Q^2}{r^2} + f(r) \left(\frac{l(l+1)}{r^2} + \mu^2 + \frac{f'(r)}{r} \right). \quad (6)$$

The tortoise coordinate r^* is defined as

$$\begin{aligned} r^* &\equiv \int \frac{1}{f(r)} dr \\ &= r + \frac{r_+^2}{r_+ - r_-} \ln(r - r_+) - \frac{r_-^2}{r_+ - r_-} \ln(r - r_-), \end{aligned} \quad (7)$$

The quasi-bound state solutions we wish to consider satisfy a purely ingoing boundary condition close to the external horizon, $R_\ell \sim e^{-i(\omega - \omega_c)r^*}$. In the far field region they should decay to zero; asymptotically these solutions can be written as $R_\ell \sim e^{\tilde{q}r}$ with $\tilde{q} = \sqrt{\mu^2 - \omega^2}$, and $\text{Re}(\tilde{q}) < 0$. As a consequence of imposing a pair of boundary conditions the spectrum of complex frequencies becomes discrete. The real part of ω sets the oscillation frequency of the mode, whereas the imaginary part determines its growth or decay rate.

III. TIME DOMAIN ANALYSIS

In order to solve the Klein-Gordon equation in the time domain, we use a more suitable coordinate system, the ingoing Kerr-Schild coordinates (t, r, θ, ϕ) , obtained from

Schwarzschild coordinates by changing the time coordinate

$$t = \tilde{t} + (r^* - r) . \quad (8)$$

In these coordinates the RN metric becomes

$$ds_{KS}^2 = - \left(1 - \frac{2M}{r} + \frac{Q^2}{r^2} \right) dt^2 + 2 \left(\frac{2M}{r} - \frac{Q^2}{r^2} \right) dt dr + \left(1 + \frac{2M}{r} - \frac{Q^2}{r^2} \right) dr^2 + r^2 (d\theta^2 + \sin^2 \theta d\phi^2) . \quad (9)$$

In terms of the standard ADM variables, $ds^2 = -(\alpha^2 - \beta^i \beta_i) dt^2 + 2\beta_i dx^i dt + \gamma_{ij} dx^i dx^j$, we read off that the lapse function α and the shift vector β^i are

$$\alpha = \left(1 + \frac{2M}{r} - \frac{Q^2}{r^2} \right)^{-1/2} , \quad \beta_r = \frac{2M}{r} - \frac{Q^2}{r^2} . \quad (10)$$

Observe that $\beta^i = [\beta_r \alpha^2, 0, 0]$. Furthermore, the radial components of the induced metric γ_{ij} are

$$\gamma_{rr} = \frac{1}{\alpha^2} , \quad \gamma_{\theta\theta} = r^2 , \quad \gamma_{\varphi\varphi} = r^2 \sin^2 \theta . \quad (11)$$

The Kerr-Schild form of the metric has become popular in the numerical relativity community because a constant t hypersurface is non singular and horizon penetrating which allows for convenient imposition of boundary conditions.

A. Scalar flux and energy

In the RN spacetime the timelike Killing vector field $k = \partial/\partial t$ defines a conserved current $J^\mu = T^\mu{}_\nu k^\nu$. The integration of the conservation law $\nabla_\mu J^\mu = 0$ over a finite region of spacetime yields

$$\int \nabla_\mu J^\mu \sqrt{-g} d^4 x = 0 . \quad (12)$$

Since the spacetime is static, the last integral becomes an integration over a surface of $t = \text{cte}$, Σ_t ,

$$\int_{\Sigma_t} \nabla_\mu J^\mu \alpha \sqrt{\gamma} d^3 x = 0 , \quad (13)$$

in terms of the standard ADM variables α and γ (determinant of the spatial metric). Taking the field energy E as the integral on a space-like slice of the zeroth component of the current

$$E = \int_{\Sigma_t} \alpha J^0 \sqrt{\gamma} d^3 x , \quad (14)$$

then (13) implies

$$\frac{d}{dt} E = - \int_{\Sigma_t} d^3 x \partial_i (\alpha \sqrt{\gamma} J^i) = - \int_{\partial \Sigma_t} \alpha J^i dS_i , \quad (15)$$

where $\partial \Sigma_t$ is the boundary of the hypersurface, $dS_i = n_i d\theta d\varphi \sqrt{g_{s^2}}$ and n^i is the vector normal.

Using the decomposition in spherical harmonics of the field (4) the energy (14), can be written as $E = \sum_{\ell, m} E_{\ell m}$, with

$$E_{\ell m} = \int_{r_+}^{\infty} \rho_\ell(r) r^2 dr , \quad (16)$$

where

$$\rho_\ell(r) = \frac{1}{2} \left[\frac{1}{\alpha^2} (|\partial_t \phi_\ell|^2 - 2q A_t \text{Im}(\phi_\ell^* \partial_t \phi_\ell)) + (1 - \beta_r) \times |\partial_r \phi_\ell|^2 + \left(\frac{q^2 A_t^2}{\alpha^2} + \frac{\ell(\ell+1)}{r^2} + \mu^2 \right) |\phi_\ell|^2 \right] .$$

In a similar way, the flux passing through a surface of $r = \text{cte}$

$$F^r \equiv - \int_{\partial \Sigma_t} \alpha J^i dS_i = - \int_{\partial \Sigma_t} T^r{}_0 r^2 d\theta d\varphi \sin \theta , \quad (17)$$

can be decomposed as a sum over angular modes, $F^r = - \sum_{\ell, m} r^2 F_{\ell m}^r$, where

$$F_{\ell m}^r = (1 - \beta_r) [\text{Re}(\partial_r \phi_\ell \partial_t \phi_\ell^*) - q A_t \text{Im}(\phi_\ell^* \partial_r \phi_\ell)] + \beta_r [|\partial_t \phi_\ell|^2 - 2q A_t \text{Im}(\phi_\ell^* \partial_t \phi_\ell) + q^2 A_t^2 |\phi_\ell|^2] .$$

B. Equations of motion

To obtain a first order system of equations of motion, we introduce the auxiliary functions

$$\psi = \partial_r \phi , \quad \pi = \frac{1}{\alpha^2} (\partial_t \phi - \beta^r \psi) , \quad (18)$$

where we have dropped the mode number subscripts to simplify the notation. The following system of evolution equations for ϕ , π and ψ is obtained.

$$\partial_t \phi = \alpha^2 (\pi + \beta_r \psi) , \quad (19)$$

$$\begin{aligned} \partial_t \psi &= \partial_r (\alpha^2 (\pi + \beta_r \psi)) \\ &= \beta^r \partial_r \psi + \alpha^2 \partial_r \pi + \frac{2r(Mr - Q^2)}{(r^2 + 2Mr - Q^2)^2} (\pi - \psi) , \end{aligned} \quad (20)$$

$$\begin{aligned} \partial_t \pi &= \beta^r \partial_r \pi + \alpha^2 \partial_r \psi \\ &- \left(\frac{\ell(\ell+1)}{r^2} - \frac{q^2 Q^2}{\alpha^2 r^2} + \mu^2 \right) \phi - \frac{2iqQ}{r} \pi + \frac{iqQ^3}{r^4} \phi \\ &+ \frac{2}{(r^2 + 2Mr - Q^2)^2} (T_1 \pi + T_2 \psi) , \end{aligned} \quad (21)$$

where

$$\begin{aligned} T_1 &\equiv \frac{1}{r} (Mr^3 + 4M^2 r^2 - 4MrQ^2 + Q^4) , \\ T_2 &\equiv r(r^2 + 3Mr - 2Q^2) . \end{aligned}$$

The definition of ψ becomes a constraint, of the form

$$C_r(r, t) = \partial_r \phi(r, t) - \psi(r, t) , \quad (22)$$

that must be satisfied at all times. If C_r is zero initially, and the evolution equation holds exactly, C_r will remain zero during the evolution. Numerical truncation errors and boundary errors may cause, however, deviations from zero. Hence, keeping track of the evolution of C_r provides a test for the accuracy of the numerical simulations.

C. Numerics and boundary conditions

The evolution equations for the radial components were solved by making use of the 1+1 dimensional PDE solver described in [24] and also used in [25]. The numerical algorithm utilized by this code is based on the method of lines in a third order Runge-Kutta scheme such that the spatial derivatives were evaluated with a second order symmetric finite difference stencil. To guarantee stability by suppressing high frequency instabilities a standard fourth order dissipation term was also applied.

We have decomposed the field into its real and imaginary part $\phi = \phi^R + i\phi^I$ and solved the corresponding system of coupled equations. The evolution scheme is simpler than for the corresponding Kerr case [14, 26]; but it is still technically challenging because of the requirement of high resolution, long integration times and boundary conditions.

A simple way to implement the mirror-like boundary condition at a given radial coordinate $r = r_m$ is by setting the field and the dynamical fields to zero at the boundary. This works well when the shift vector is equal to zero. For the RN spacetime in Kerr-Schild coordinates, however, this boundary condition produces strong violations of the constraint. These constraint violations propagate into the inner domain and grow, eventually dominating the numerical solution.

In order to impose the mirror-like boundary condition in our numerical scheme we proceed as follows. At the mirror position the field must satisfy three conditions $\phi(r_m) = 0$, $\partial_t \phi(r_m) = 0$ and $\partial_{tt} \phi(r_m) = 0$. The first condition is straightforward to implement. The second, using equation (19) gives a relationship between $\psi(r_m)$ and $\pi(r_m)$. For the third we substitute the definition of π , $\partial_{tt} \phi(r_m) = \partial_t(\alpha^2 \pi(r_m) + \beta^r \psi(r_m)) = \alpha^2 \partial_t \pi(r_m) + \beta^r \partial_t \psi(r_m)$ and use the equation (21) together with (20) to get an equation for $\pi(r_m)$, $\psi(r_m)$ and their spatial derivatives. Finally we use one sided finite differencing stencils to approximate the radial derivatives. This procedure provide us an algebraic system of equations for $\psi(r_m)$ and $\pi(r_m)$ in terms of their values at the inner points that has to be solved at each time step.

IV. RESULTS

Solving the above system of equations of motion one obtains a time series for the scalar field amplitude at an observation point with a given radius r_o , with $r_+ < r_o < r_m$. After a given number of time steps we perform a Fast Fourier transform to obtain the field amplitude in frequency space - the power spectrum - and identify the frequencies. In the following we shall report two distinct cases. The evolution of the charged scalar field in 1) the asymptotically Minkowski RN BH; 2) in the RN BH in a cavity.

A. Asymptotically Minkowski space

We have evolved the charged scalar field in the RN background *without* imposing the mirror-like boundary condition. Instead, we impose the condition $\pi + \psi = 0$ at some $r = r_{max}$. For an uncharged massless scalar this corresponds to impose the incoming characteristic modes to be zero. For a charged massive scalar field this condition introduces a small error that propagates inside the numerical domain. In order to avoid any kind of contamination we set r_{max} sufficiently far out, i.e $r_{max} > t_{evol}$ where t_{evol} is the total evolution time.

Fig. 1 (left panel) illustrates a generic evolution. We have used as initial data at $t = 0$ a static Gaussian perturbation centered at r_{cg} :

$$\phi(r, 0) = \phi_0 e^{-(r-r_{cg})^2/2\sigma^2} , \quad \partial_t \phi(r, 0) = 0 , \quad (23)$$

with $\phi_0 = 3 \times 10^{-3}$, $r_{cg} = 10M$ and $\sigma = 2M$. The power spectrum obtained from this time evolution data, shows set of distinct frequencies that can be compared with those obtained in the frequency domain in [16, 27] for the same parameters. This comparison is made in Table I and shows a good agreement.

Q/M	qM	$\text{Re}(M\omega)_{Analytical}$	$\text{Re}(M\omega)_{Numerical}$
0.1	0.1	0.2875	0.287
0.1	0.5	0.2900	0.290
0.6	0.1	0.2903	0.290
0.6	0.4	0.2993	0.299

TABLE I: Comparison between analytic and numerical frequencies for the same parameters as in Fig. 1. The analytic (numerical) ones were obtained using the continued fraction method (Fourier transform of the evolution data).

A curious behaviour that can be observed in the asymptotically flat case, due to the absence of growing modes is displayed in Fig. 1 (right panel). When the initial data excites two modes with a similar frequency, one observes a *beating* behaviour. This has already been

noticed in [14] for an uncharged field in a rotating background and in [28] in a Schwarzschild background. This beating results from the coupling between the two modes

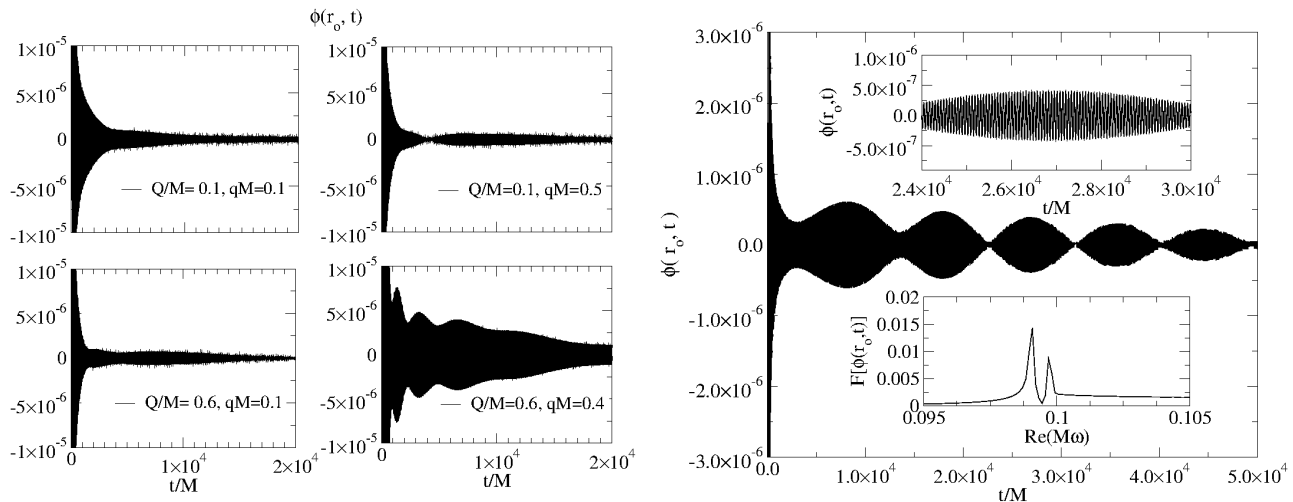


FIG. 1: Evolution of the scalar amplitude for a spherical ($\ell = 0$) Gaussian perturbation with $\phi_0 = 3 \times 10^{-3}$, $r_g = 10M$, $\sigma = 2M$. (Left panel) Decaying patterns for $r_o = 10M$, $M\mu = 0.3$ and various values of Q, q . M was set to one in the figure. (Right panel) Beating pattern obtained for $r_o = 70M$, $M\mu = 0.1$, $Q/M = 0.1$ and $Mq = 0.3$. The upper inset is a zoom showing the oscillating behaviour; the Fourier transform is shown in the bottom inset and exhibits the two excited modes.

B. RN BH in a cavity

Gaussian initial data

We consider a Gaussian initial data, described by eq. (23). Unless otherwise specified we take $r_m = 15M$, $r_o = 5M$, $\mu M = 0.1$. For some values of the parameters the evolution is displayed in Fig. 2. This figure shows that at early times, $t/M \lesssim 10^4$, the field amplitude (top left panel) decreases; but an exponential growth follows. The exponential growth becomes clear in the left bottom panel of Fig. 2, where the field energy is displayed against a linear fit of the form $\ln(E/E_0)$ as a function of t/M (blue dashed line). In the inset, the initial decrease of the field energy due to the absorption by the BH is shown. The right panels of Fig. 2 show the power spectrum of the Fourier transform of the field amplitude obtained at four different stages in the evolution and provide a mode interpretation of the field's development. At stage 1 ($t/M = 10^3$) one identifies three well resolved frequencies. The dominant mode is the first overtone which has an exponential decay. The critical frequency, separating growing modes ($\omega < \omega_c$) from decreasing modes ($\omega > \omega_c$) is $\omega_c = 0.501431$ and it is marked with a vertical dashed line. At stage 2 ($t/M = 10^4$) one observes a noticeable growth of the fundamental mode which becomes compa-

with similar frequency which can be observed in the inset of the figure.

able to the first overtone at stage 3 ($t/M = 4 \times 10^4$). Finally, at stage 4 ($t/M = 2 \times 10^5$), the dominant mode is the fundamental mode. The exponential growth rate for the energy corresponding to the dashed blue line in the bottom left panel is in agreement with twice the imaginary part of the frequency of the fundamental mode with an error of less than 1%.

Next we compare time evolutions for different values of the field charge q , keeping the same Gaussian initial data as before. We take three cases with $qM = 0.8, 1.0, 1.2$, keeping $Q/M = 0.9$ and considering modes with $\ell = 1$; the frequencies of the fundamental mode and first two overtones are displayed in Table II. Observe that the unstable modes are the ones with a positive imaginary part.

In Fig. 3 we display the time evolution of the field amplitude (left panels) and power spectrum of the Fourier transform (middle panels) for the three cases described in the previous paragraph. In all three cases the field amplitude grows exponentially. The power spectrum, taken at $t/M = 1.5 \times 10^5$, shows that the dominant mode is always the one with the largest (positive) imaginary part in Table II, that is, the fastest growing mode. The right panel of Fig. 3 shows an exponential growth for the field energy that matches twice the imaginary part of the frequency of the corresponding fastest growing mode.

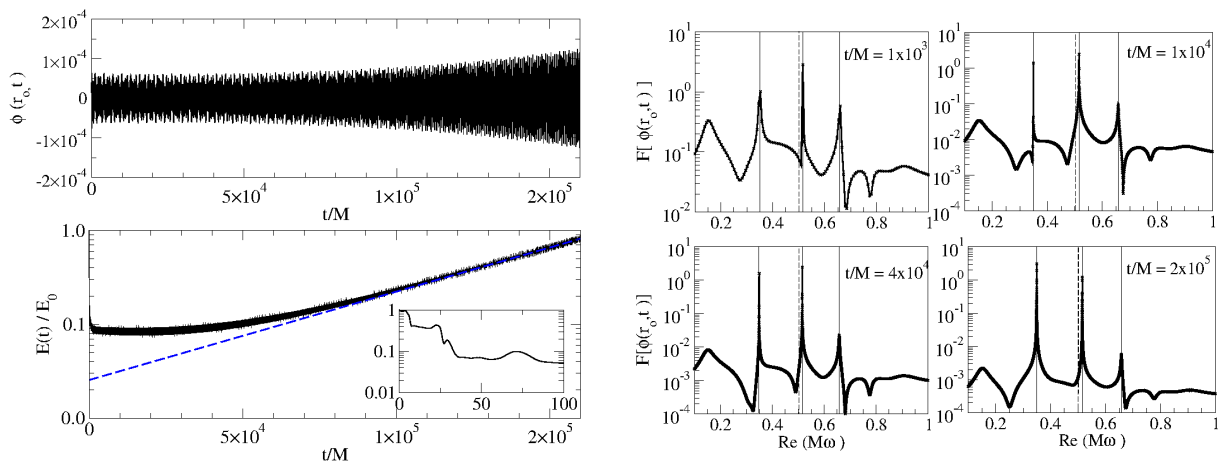


FIG. 2: Evolution of a Gaussian wave packet with $r_{cg} = 7M$, $\sigma = M$ and $\phi_0 = 3 \times 10^{-4}$ for a field mode with $\ell = 1$, $qM = 0.8$ and a background with $Q/M = 0.9$. The top left panel shows the field amplitude. The left bottom panel displays the field energy and the inset details the initial loss of energy in the field, due to BH absorption. The right panels show the power spectrum of the Fourier transform of the field amplitude at four different time stages.

n	$Mq = 0.8$	$Mq = 1.0$	$Mq = 1.2$
0	$0.349348 + 1.084 \times 10^{-5}i$	$0.369909 + 2.2807 \times 10^{-5}i$	$0.390017 + 4.300 \times 10^{-5}i$
1	$0.515418 - 7.66693 \times 10^{-6}i$	$0.542963 + 2.7655 \times 10^{-5}i$	$0.569346 + 5.469 \times 10^{-5}i$
2	$0.65799 - 1.3986 \times 10^{-3}i$	$0.694465 - 1.94583 \times 10^{-4}i$	$0.727795 + 2.905 \times 10^{-5}i$

TABLE II: Complex frequencies for three first mirrored states taking $Q/M = 0.9$, $\ell = 1$.

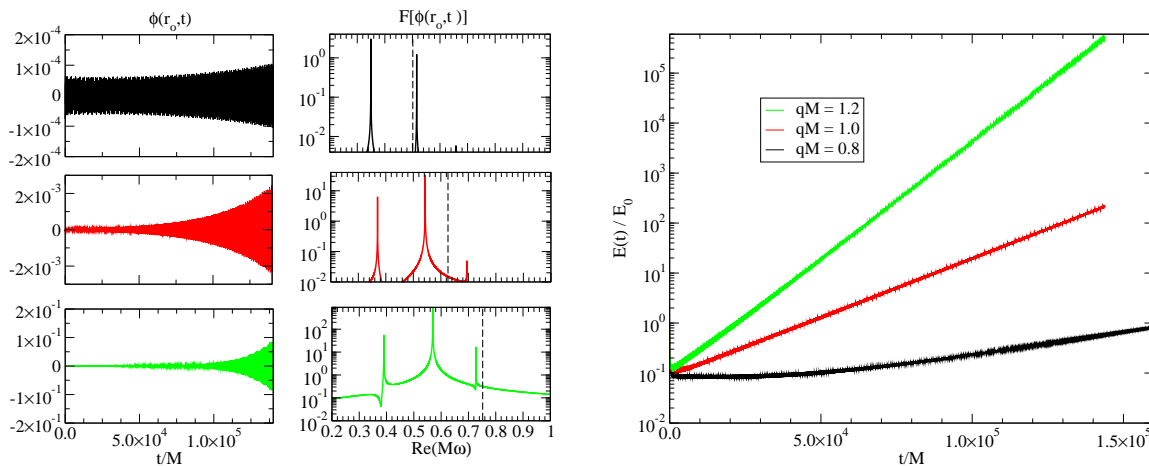


FIG. 3: (Left panels) Time evolution of the field amplitude for, from top to bottom, $Mq = 0.8, 1.0, 1.2$, $Q/M = 0.9$ and $\ell = 1$. (Middle panels) Fourier transform of the times series data. The dashed lines mark the critical frequencies $M\omega_c = 0.501431$, $M\omega_c = 0.626789$, $M\omega_c = 0.752147$. (Right panel) Normalized energy.

We also consider the evolution of $\ell = 0$ modes to show they exhibit the superradiant instability and compare their growth time rates with the $\ell = 1$ modes. Super-

radiant $\ell = 0$ modes are particular to charged BHs, and do not occur in the rotating case. For the same q, Q parameters as before we find that the frequencies of the

fundamental mode and first two overtones are those displayed in Table III. Then, in Fig. 4 the time evolution of these modes is displayed in analogy to Fig. 3. A notice-

able fact is that the growth rates are about two orders of magnitude faster than the corresponding $\ell = 1$ modes.

n	$Mq = 0.8$	$Mq = 1.0$	$Mq = 1.2$
0	$0.28936 + 2.10503 \times 10^{-3}i$	$0.31285 + 2.78491 \times 10^{-3}i$	$0.33541 + 3.43661 \times 10^{-3}i$
1	$0.44594 + 0.63712 \times 10^{-3}i$	$0.47943 + 2.75014 \times 10^{-3}i$	$0.51008 + 3.44575 \times 10^{-3}i$
2	$0.57591 - 8.47143 \times 10^{-3}i$	$0.62207 + 2.80632 \times 10^{-4}i$	$0.66325 + 2.83061 \times 10^{-3}i$

TABLE III: Complex frequencies for the three first mirrored states taking $Q/M = 0.9$, $\ell = 0$.

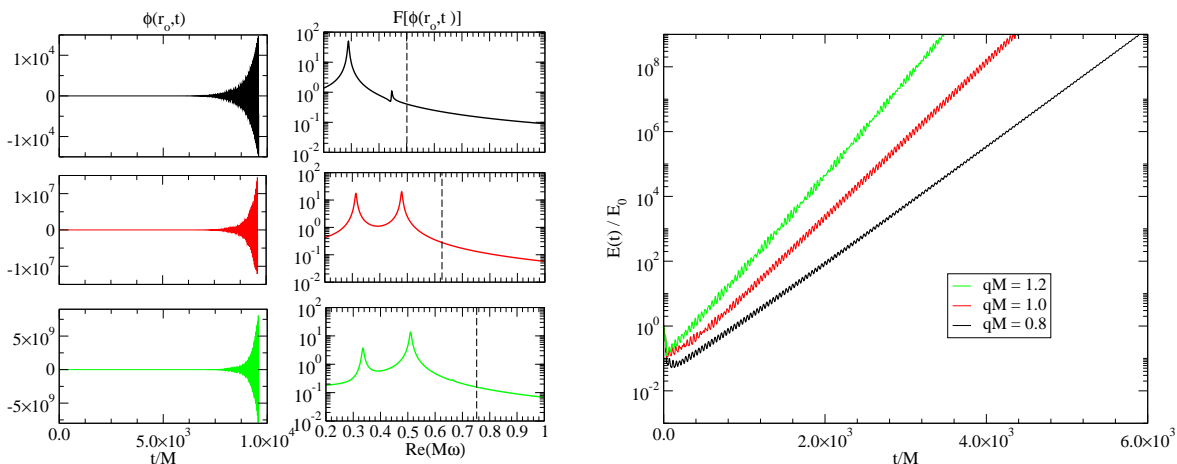


FIG. 4: (Left panels) Time evolution of the field amplitude for, from top to bottom, $Mq = 0.8, 1.0, 1.2$, $Q/M = 0.9$ and $\ell = 0$. (Middle panels) Fourier transform of the times series data. The dashed lines mark the critical frequencies $M\omega_c = 0.501431$, $M\omega_c = 0.626789$, $M\omega_c = 0.752147$. Note that critical frequencies are ℓ -independent. (Right panel) Normalized energy.

Regularized mirrored states

The previous examples with Gaussian initial data, as well as other numerical experiments, show that for a given set of parameters q, μ, Q, ℓ, r_m , the corresponding fundamental mode and the first overtones are excited. Perhaps all overtones are excited, but for higher overtones, which are energetically more costly, the corresponding amplitude is too small to be seen in our numerical evolutions. One may ask, however, if it is possible to choose initial data as to excite a *single* frequency. The obvious initial data to attempt such state, is to take the radial function of the mirrored state. These radial functions obey eq. (5) and may be constructed in the

frequency domain [16]. We have consider the time evolution of such an initial state: the fundamental mode for $qM = 0.9 = Q/M$, $\ell = 1$. The Fourier transform of the time evolution of the field's amplitude is shown in Fig. 5. We observe that higher overtones appear excited as well. The reason may be related to the fact that mirrored states (as in the generic case of quasi-bound states) diverge at the event horizon and the radial function we have used to mimic the quasi-bound state is smoothed out therein. Although the two radial functions only differ in a small vicinity of the horizon this may be enough to excite other states.

Rapid growth configurations

Finally we shall consider the fastest growing config-

urations discussed in [16]. We thus take $r_m = 5M$, $qM = 40$, $Q/M = 0.9$ and $\ell = 1$ for which a mode

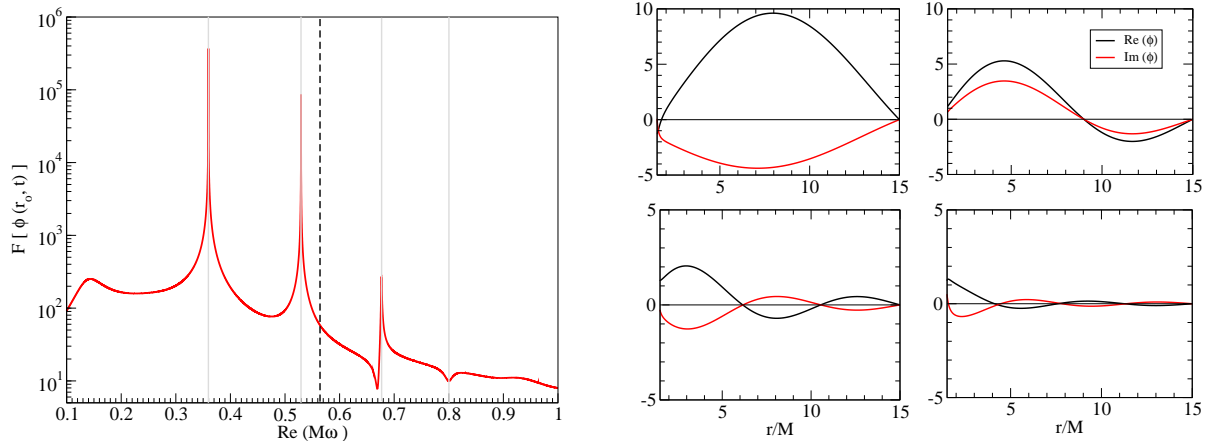


FIG. 5: (Left panel) Fourier transform of the field amplitude for a regularized mirrored state: the fundamental mode for $\ell = 1, Q/M = 0.9, qM = 0.9$. The critical frequency is $M\omega_c = 0.56411$ (dashed line). The vertical lines denote the first overtones obtained with direct integration of the radial equation. (Right panel) Real and imaginary part of the ground state of the field and the first 3 overtones.

was reported with $M\omega = 9.4655 + 0.07099i$. For the same parameters the most unstable mode with $\ell = 0$ has $M\omega = 9.4385 + 0.08157i$. Thus for this values of the charge the difference in growth rate for $\ell = 0$ and $\ell = 1$ modes has already become very small. We checked this is the general pattern: as q increases the dependence in ℓ becomes less important in agreement with the results of [22]. Fig. 6 shows the signal as measured by an observer located at $r_o = 3M$. As in the previous cases we took a Fourier transform of the signal to obtain the oscillating frequency. In this high frequency set up the dominant mode is the ground state. At very early times one can see the growth of the signal. Although we do not have enough data to say whether other overtones are present (longer runs will drive the energy very outside of the test field regime) the frequency agrees with the value previously reported. The growth rate coincides with the imaginary part of the frequency as well.

V. CONCLUSIONS

The laws of BH mechanics do not forbid physical processes that may extract energy from BHs. Indeed, for a Kerr-Newman BH, the first and second laws require only that the BH energy variation dE is bounded below by the angular momentum and charge variations, dJ, dQ respectively, as

$$dE \geq \Omega_H dJ + \Phi_H dQ .$$

Thus energy extraction, i.e $dE < 0$, is possible if accompanied by a sufficient large extraction of either angular momentum or charge. A physical process that materializes this possibility is superradiant scattering. Taking $dE = -\omega$, $dJ = -m$, $dQ = -q$ one obtains precisely the superradiance conditions described in the Introduction.

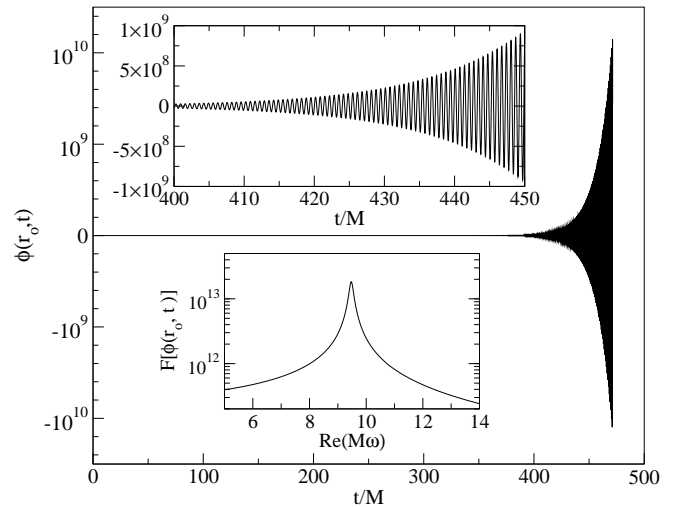


FIG. 6: Rapid growing mode. The parameters are $\ell = 1, Q/M = 0.9, qM = 40$. The main panel shows the signal amplitude. The upper inset is a zoom to show the oscillating behaviour. The Fourier transform is shown in the bottom inset.

The existence of quasi-bound states of a bosonic field in the superradiant regime generates an instability of the BH. The field extracts energy from the BH, together with angular momentum and charge (or both), and starts to pile up around it until non-linear phenomena start to dominate the evolution. Understanding such evolution requires non-linear numerical simulations. Some progress in this type of simulations for the Kerr case has been reported in [8, 29], where non-linear interactions for the

scalar field were considered but not the backreaction on the geometry. The fully-non linear system for the coupled Einstein-scalar field equations seem quite challenging for this case. Even though the numerical relativity community has available techniques to tackle such problems [9], the very slow growth rates require very long time evolutions, and above all, preventing numerical errors from masking the physical signal.

In this paper we have reported linear time evolutions for a charged scalar field in the background of a RN BH and in particular observed the superradiant growth - in the linear regime - of the field when the BH is enclosed in a cavity. Our results further confirm the existence of rapid growing unstable modes - as compared to the Kerr case - and which may be spherically symmetric [16]. These two features provide a considerable advantage in

performing fully non-linear numerical simulations. Such simulations will allow monitoring the development and understanding the end-point of the superradiant instability in a setup which, albeit not exactly equal, will share common features to the astrophysically more relevant Kerr case.

Acknowledgements

J. C. D. acknowledges support from CONACyT-México and from FCT via project No. *PTDC/FIS/116625/2010*. This work was also supported by the *NRHEP295189 FP7-PEOPLE-2011-IRSES* Grant.

-
- [1] J. M. Bardeen, W. H. Press, and S. A. Teukolsky, *Astrophys.J.* **178**, 347 (1972).
 - [2] A. A. Starobinsky, *Zh. Eksp. Teor. Fiz.* **64**, 48 (1973).
 - [3] W. H. Press and S. A. Teukolsky, *Nature* **238**, 211 (1972).
 - [4] T. Zouros and D. Eardley, *Annals Phys.* **118**, 139 (1979).
 - [5] V. Cardoso, O. J. Dias, J. P. S. Lemos, and S. Yoshida, *Phys.Rev.* **D70**, 044039 (2004), hep-th/0404096.
 - [6] S. R. Dolan, *Phys.Rev.* **D76**, 084001 (2007), 0705.2880.
 - [7] V. Cardoso, (2013), 1307.0038.
 - [8] H. Yoshino and H. Kodama, *Prog.Theor.Phys.* **128**, 153 (2012), 1203.5070.
 - [9] V. Cardoso *et al.*, *Class.Quant.Grav.* **29**, 244001 (2012), 1201.5118.
 - [10] E. Berti, V. Cardoso, and A. O. Starinets, *Class.Quant.Grav.* **26**, 163001 (2009), 0905.2975.
 - [11] S. Hod and O. Hod, *Phys.Rev.* **D81**, 061502 (2010), 0910.0734.
 - [12] J. Rosa, *JHEP* **1006**, 015 (2010), 0912.1780.
 - [13] P. Pani, V. Cardoso, L. Gualtieri, E. Berti, and A. Ishibashi, *Phys.Rev.Lett.* **109**, 131102 (2012), 1209.0465.
 - [14] H. Witek, V. Cardoso, A. Ishibashi, and U. Sperhake, *Phys.Rev.* **D87**, 043513 (2013), 1212.0551.
 - [15] S. R. Dolan, (2012), 1212.1477.
 - [16] C. A. R. Herdeiro, J. C. Degollado, and H. F. Runarsson, *Phys.Rev.* **D88**, 063003 (2013), 1305.5513.
 - [17] J. Bekenstein, *Phys.Rev.* **D7**, 949 (1973).
 - [18] H. Furuhashi and Y. Nambu, *Prog.Theor.Phys.* **112**, 983 (2004), gr-qc/0402037.
 - [19] S. Hod, *Phys.Lett.* **B713**, 505 (2012).
 - [20] S. Hod, *Phys.Lett.* **B718**, 1489 (2013).
 - [21] R. Konoplya and A. Zhidenko, (2013), 1307.1812.
 - [22] S. Hod, *Physical Review D* **88**, **064055** (2013), 1310.6101.
 - [23] H. Witek *et al.*, *Phys.Rev.* **D82**, 104037 (2010), 1004.4633.
 - [24] J. C. Degollado, D. Nunez, and C. Palenzuela, *Gen.Rel.Grav.* **42**, 1287 (2010), 0903.2073.
 - [25] J. Barranco *et al.*, *Phys.Rev.* **D84**, 083008 (2011), 1108.0931.
 - [26] M. J. Strafuss and G. Khanna, *Phys.Rev.* **D71**, 024034 (2005), gr-qc/0412023.
 - [27] J. C. Degollado and C. A. Herdeiro, *Gen.Rel.Grav.* **45**, 2483 (2013), 1303.2392.
 - [28] J. Barranco *et al.*, In preparation .
 - [29] H. Yoshino and H. Kodama, (2013), 1312.2326.